

Hydrogen and deuterium in epitaxial Y(0001) films: Structural properties and isotope exchange

A. Remhof, G. Song, Ch. Sutter, A. Schreyer, R. Siebrecht, and H. Zabel

Ruhr-Universität Bochum, Institut für Experimentalphysik/Festkörperphysik, D-44780 Bochum, Germany

F. Güthoff and J. Windgasse

Forschungszentrum Jülich, Institut für Festkörperforschung, D-52425 Jülich, Germany

(Received 15 October 1998)

Hydrogen in yttrium is of fundamental interest as a model system for driving metal-insulator transitions including switchable optical properties from reflecting to transparent in the visible region. We report on the structural properties of hydrogenated and deuterated thin, monocrystalline Y(0001) films grown by molecular beam epitaxy on Nb/Al₂O₃ substrates. X-ray diffraction reveals the response of the host metal lattice upon hydrogen loading. The structural coherence in all three spatial directions as well as the epitaxial relation to the substrate are maintained, though the sample undergoes structural phase transitions between the different hydride phases. With neutron reflectivity measurements we have determined the hydrogen and deuterium content since the critical angle for total reflection depends on their concentration in the sample. Measurements on hydrogenated and deuterated films show that H and D are completely interchangeable within the trihydride phase. Neutron scattering also allows us to determine the position of the deuterium atoms within the yttrium matrix. All structural information gained on thin films is in agreement with the space group $P\bar{3}c1$ which was previously determined from powder samples. [S0163-1829(99)02810-6]

I. INTRODUCTION

Within the past decades the properties of hydrogen in metals and alloys have been studied in much detail.¹⁻³ Recent advances in thin film deposition techniques and hydrogen loading capabilities caused renewed interest in metal-hydrogen systems. Exciting structural and functional properties have been discovered in recent years stimulating further work on thin films and superlattices. Among those are hydrogen induced changes of the exchange coupling in Fe/Nb (Ref. 4) and Fe/V (Ref. 5) superlattices, giant lattice expansions caused by hydrogen in Mo/V (Ref. 6) superlattices, and an extraordinary adhesion of Nb on sapphire substrates as probed by the hydrogen induced lattice expansion.⁷ These results indicate that hydrogen in metals is more than a structural ingredient and can be used as a functional agent in high technology materials.

Among different hydrogen-metal systems, rare earth (RE) metals and their chemical relatives Sc, Y, and La are of special interest because of their ability to absorb up to three hydrogen atoms per metal atom.

The phase diagram of the RE-H systems consists of three principle phases depending on the hydrogen concentration.⁸ At low concentrations (α -phase), hydrogen in RE metals can be described as a lattice gas where the hydrogen atoms are distributed on interstitial sites of the host lattice with tetrahedral symmetry. In yttrium the solubility limit of the α phase is $x=0.2$ at room temperature ($x=H/Y$). Within this solid solution phase the Y remains metallic. At higher concentrations, stable dihydride (β) and trihydride (γ) phases form. While most RE metals crystallize in the hcp structure, all dihydrides of trivalent RE metals transform to a CaF₂-like cubic structure in which all tetrahedral interstitial sites of the fcc metal lattice are filled with hydrogen. This structural transformation consists of an expansion of the metal lattice

along the c axis by typically 5%. The expansion is accompanied by a rearrangement of the stacking sequence. The formally $ABAB$ stacked hexagonal basal planes become an $ABCABC$ stacked cubic closed packed crystal. Apart from the divalent lanthanides and from the systems La-H, Ce-H, and Pr-H, which retain their cubic symmetry, all RE undergo a second phase transition at higher H concentrations to the hexagonal γ phase. Within the γ phase the metal atoms regain their $ABAB$ stacking sequence, while the closed packed planes are even further pushed apart, resulting in a c axis expansion of about 15%.

For yttrium and the heavy rare earth, the dihydride phase has metallic properties which gradually disappears as the system approaches the trihydride phase. The exact phase boundaries of the α phase in the RE is difficult to study because of the very high solution enthalpy.

For the β and γ phase reliable phase boundaries are scarce. Only for Y the phase boundaries have recently been investigated using thin film techniques.⁹

Several unusual properties have been found in RE-H_x systems such as pairing¹⁰ and rapid low-temperature hopping of hydrogen¹¹ within the solid solution phase as well as a metal-semiconductor transition within the dihydride phase.¹² Most recently, hydrogen governed switching of the optical properties in YH_x and LaH_x thin polycrystalline films have been observed within the trihydride phase.⁹ In the trihydride phase, the formerly reflecting metallic film becomes transparent. The optical changes are accompanied by a metal-insulator transition at hydrogen concentrations above $x=2.8$. The film can reversibly be loaded with hydrogen and the switching time between a metallic reflecting mirror and a transparent film is on the order of a fraction of a second.¹³ Recently, single crystalline films of YH₃ and YH₂ have been prepared by controlled hydrogen loading of molecular beam epitaxy (MBE) grown yttrium films.¹⁴ The transformation

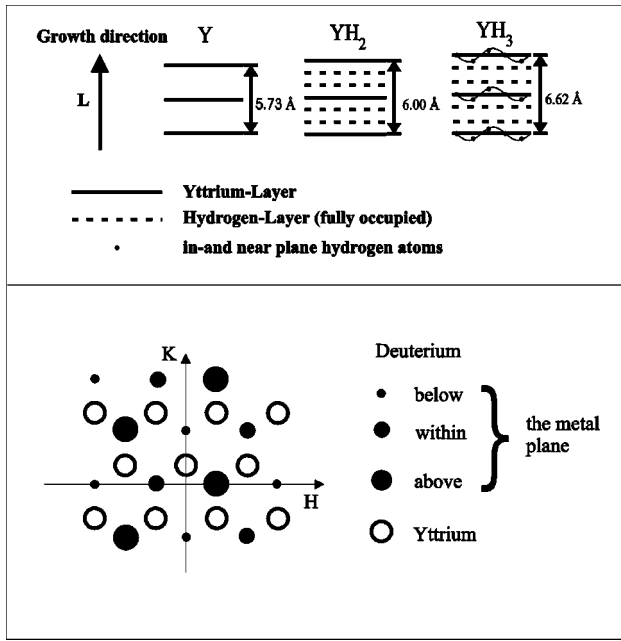


FIG. 1. The upper panel shows the layered structure of Y, YH₂, and YH₃ along the *c* axis. The lower panel gives a top view of the hexagonal basal plane of YH₃. Using three independent indices, the (11 $\bar{2}$ 0) direction will be called H while K labels the (10 $\bar{1}$ 0) direction. Perpendicular to H and K, L denotes the growth direction.

between the dihydride and the trihydride phase did not effect the quality of the crystal in the direction normal to the surface, i.e., the growth direction. Furthermore, this structural transition is completely reversible without any loss of structural coherence.¹⁴ However, the optical switching time is considerably longer for the epitaxial films as compared to the polycrystalline films.

In this paper we will focus on the structure of YH₃ and the epitaxial relation between Y and YH₃ on Nb/Al₂O₃ substrates in single crystalline films as revealed by x-ray and neutron scattering.

In previous neutron powder diffraction (NPD) work, Udovic *et al.* have determined the positions of the hydrogen atoms within the hcp phase of YD₃.¹⁵ The structure has the space group $P\bar{3}c1$. In this structure the D atoms occupy unusual interstitial sites. hcp lattices offers two kinds of high symmetry interstitial sites with octahedral (O) and tetrahedral (T) symmetry. Per metal atom there are two T sites and one O site. In YD₃, the deuterium atoms occupying the O sites are shifted parallel to the *c* axis towards the basal metal plane. An additional wavelike modulation displaces one third of the O sites above the metal plane and one third below the metal plane, while the basal metal plane hosts the remaining third. The T sites are also slightly displaced from their conventional positions in a correlated manner. The resulting distribution of D atoms parallel to the Y(0001) axis of YD₃ can be described as consisting of a regular stack of D layers schematically indicated in Fig. 1(a). Between any two consecutive yttrium planes (solid lines) four deuterium planes are arranged. The two planes with tetrahedral site symmetry are fully occupied as in the YD₂ phase (dashed lines). The wavelike modulation of the deuterium atoms occupying the octahedral sites close to the metal plane results in three more

planes which are each filled by one third of the remaining deuterium atoms (wavy line). Later we will refer to those planes as in and near metal planes. Figure 1(b) shows a top view on a basal plane. The hydrogen modulation can be considered as a transverse modulation with propagation in the [11 $\bar{2}$ 0]-like directions, which we will call H later on. The perpendicular [1 $\bar{1}$ 00]-like directions will be referred to as K direction when using three independent indices [HKL] to describe the lattice in more convenient terms. Details of this structure are given by Udovic *et al.*¹⁵

First-principles total-energy calculations carried out by Wang and Chou for YH₃ (Ref. 16) showed that the YD₃ structure as described above is the energetically most stable crystal structure. Although the structure of YH₃ seems to be known, standard local density approximation calculations fail to predict the metal insulator transition.^{17,18}

The insulating state of LaH_{2+x}, which also undergoes a metal insulator transition, has recently been explained by Ng *et al.*¹⁹ in a local model assuming localized states centered at vacancies in the RE-H₃ structure. In another density functional approach by Kelly *et al.*²⁰ small symmetry lowering displacements of the hydrogen atoms are required for driving the metal-insulator transition and for opening a band gap. In both models the main challenge is to understand why only minute structural changes induced either by vacancies or by collective displacements cause dramatic changes within the electronic configuration.

Both models use the lattice symmetry determined from polycrystalline or powder samples, whereas most of the effects mentioned above have been discerned for thin films and superlattices. In epitaxially grown films the assumption of bulk symmetry is not necessarily correct. Pseudomorphic growth and clamping effects to the substrate during hydrogen uptake may change the symmetry. For a better understanding of the structural properties and their relation to the electronic properties it is therefore necessary to study single crystalline RE films with varying hydrogen concentration. Because of the structural phase transitions mentioned above, it is not clear whether the once deposited epitaxial RE film would maintain its structural integrity up to $x=3$. According to Vajda,⁸ in the past single-crystal work on hydrides was limited to the system CeH_{2+x}. In all other RE hydrides the transformation from hcp to fcc leads to a loss of monocrystallinity. As we will show, epitaxially grown Y(0001) films on Nb/Al₂O₃ substrates maintain their structural coherence and their bulk symmetry during hydrogen loading. There is no loss of crystallinity during the transition from YH₂ to YH₃. The transition is completely reversible and can be cycled for many times. Neutron diffraction data on the deuterated films are in agreement with NPD data, indicating matching structural properties for epitaxially grown thin films and powder samples. Furthermore it is possible to completely exchange H against D within the trihydride phase on a very short time scale.

II. EXPERIMENTAL CONDITIONS

A. Sample preparation

The samples were prepared via molecular beam epitaxy in a Riber EVA 32 MBE evaporation chamber. We evaporated

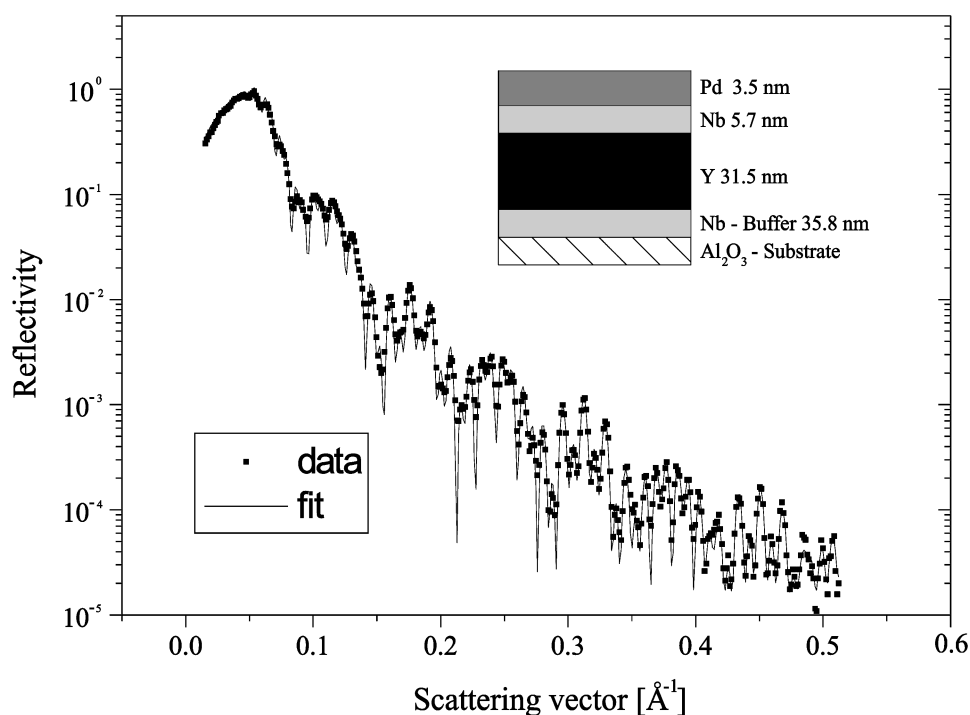


FIG. 2. Small angle x-ray reflectivity of an epitaxially grown Y film and a fit to the data points. The inset shows the sample architecture. The film thicknesses result from the fit. The interface roughnesses lie below 5 Å.

Y(0001) films with a typical thickness of 300 Å on Al_2O_3 (11 $\bar{2}$ 0) substrates. The Y film is separated from the sapphire substrate by a Nb(110) buffer to prevent chemical reactions with the substrate. To protect the Y film from oxidation and to dissociate the hydrogen molecules at the surface, the sample was covered with a thin Pd cap layer. However, palladium does not wet the Y(0001) surface well and tends to form islands, defeating its purpose. Therefore we deposited a second niobium film of about 60 Å thickness on the Y(0001) surface prior to the Pd growth to enhance the layer growth and the oxide protection. This procedure is only necessary for epitaxially grown Y(0001) films and appears not to be required for polycrystalline Y films. The resulting sample architecture is shown in the inset of Fig. 2. The layer thicknesses are results from the fit to small x-ray scattering experiments to be discussed in the next section.

Hexagonal closed packed RE metals are known to grow epitaxially on cubic Nb.²¹ The most densely close-packed Y(0001) planes grow on the most densely close-packed Nb (110) planes. The epitaxial relation follows the Nishiyama-Wassermann orientation, where the (1 $\bar{1}$ 00) axes of the hcp RE is parallel to the ($\bar{1}$ 10) axes of the bcc Nb. In the special case of Y on Nb there is a 3:4 match, i.e., a supercell commensuration between the Y(1 $\bar{1}$ 00) distances of 3.16 Å and the Nb($\bar{1}$ 10) distances of 2.34 Å. As the supercell commensuration is not perfect, we see a slight in-plane compression and a slight out-of-plane elongation in c axis grown films. While Y grows in one single domain on niobium, niobium tends to form domains when evaporated on yttrium which are rotated against each other by 120°. This is caused by the hexagonal symmetry of the (0001) grown yttrium surface. Since the hydrides also form hexagonal basal planes with corresponding lattice spacings of 3.184 Å (YH₂) and 3.177 Å (YH₃), they should obey the same epitaxial relation on the Nb(110) substrate.

During the growth process, *in situ* reflection high-energy electron diffraction (RHEED) was performed, confirming the excellent interface quality of the samples. Further details of the metal deposition and the experimental set-up are provided in Ref. 14.

B. X-ray scattering

X-ray scattering is not sensitive to the hydrogen, however, it allows to characterize the host metal films and to study their response to the hydrogen uptake. Structural characterizations along the growth direction were performed via high angle x-ray scattering using Mo $K_{\alpha 1}$ radiation of a fine focus x-ray tube. The thicknesses of the individual layers within the sample were determined by small angle x-ray reflectivity measurements. Grazing incident x-ray diffraction (GIXRD) was carried out employing Cu K_{α} radiation from a rotating anode x-ray generator. The resolution of the instrument allows to determine lattice parameters with an accuracy of about 0.002 Å. For the *in situ* studies of the structural changes under hydrogen loading a x-ray furnace with Kapton windows was used.

In the high angle regime, scans in two different directions of the reciprocal space were carried out. Rocking scans, i.e., transverse scans perpendicular to the scattering vector, reveal the mosaicity of the sample. In radial or longitudinal scans along the scattering vector lattice constants and the structural coherence lengths are determined.

C. Neutron scattering

In contrast to x-ray scattering, neutron scattering is sensitive to the presence of hydrogen in the sample and is able to distinguish between the different hydrogen isotopes via their different scattering lengths. Therefore, additional information about the actual positions of the hydrogen atoms and the hydrogen concentration in the yttrium film can be gained. In

small angle neutron reflectivity measurements the position of the critical angle for total reflection depends sensitively on the hydrogen concentration and the isotope chosen.²² At high angles the periodic modulation of deuterium atoms gives rise to additional Bragg reflections which cannot be seen using x rays. The structure factors of the individual Bragg reflections depend explicitly on the H or D concentration. Comparing the relative intensities for YH_3 and YD_3 (0002) reflections it is thus possible to analyze the position and the occupancy of the hydrogen layers in the direction along the film normal.

The neutron reflectivity experiments as well as the isotope exchange were carried out at the reflectometer ADAM (advanced diffractometer for the analysis of materials) at the Institute Max von Laue Paul Langevin (ILL) in Grenoble/France. ADAM is a fixed wavelength two circle instrument. It is connected to a liquid deuterium cold source of the ILL reactor. A focusing HOPG monochromator at a fixed take off angle of 82° selects neutrons with a wavelength of $\lambda_0 = 4.4 \text{ \AA}$. A Be filter removes $\lambda_0/2$.²³ Although ADAM was primarily designed as a reflectometer in the small angle regime, it covers a 2θ range up to 140° , accessing scattering vectors \mathbf{Q} up to 5.4 \AA^{-1} when using $\lambda_0/2$. ADAM offers the unique opportunity to perform small angle reflectivity measurements as well as high angle Bragg scattering without changing the sample environment or the alignment of the instrument.

Off-specular rods were measured at the thermal triple-axis spectrometer UNIDAS at the neutron research reactor DIDO in the Forschungszentrum Jülich in Jülich, Germany. The double monochromator system, consisting of two identical, vertical focusing pyrolytic graphite (002) crystals, allows to select incident wavelength between 0.8 \AA and 4 \AA . After interaction with the sample the neutrons can be analyzed in energy and direction with an analyzer crystal [pyrolytic graphite (002)] and a ^3He detector. During the experiments the wavelength of the incident neutrons was kept constant at 2.3558 \AA . The analyzer was used to select the elastically scattered neutrons from the sample, reducing the background.

In both neutron experiments, the sample was mounted vertically, i.e., the surface normal lying in the horizontal scattering plane. A vacuum chamber with an Al window was used for scattering experiments with *in situ* hydrogen loading capabilities.

III. RESULTS AND DISCUSSION

A. X-ray scattering characterization of the hydrogen free sample

Figure 2 shows an x-ray reflectivity scan of a representative sample before hydrogen loading. The solid line represents a fit to the data points using a modified Parratt formalism including interfacial roughness.^{24,25} Typical interface roughnesses lie below 5 \AA . The thickness parameters resulting from the fit are shown in the inset of Fig. 2. A high angle radial scan of the Y(0002) reflection is reproduced in Fig. 3. The main Bragg peak is accompanied by finite size oscillations. The longitudinal width and the position of the finite size oscillations correspond to a coherently grown film thickness of 309 \AA , which agrees very well with the layer thickness as deduced from the reflectivity data in Fig. 2. There-

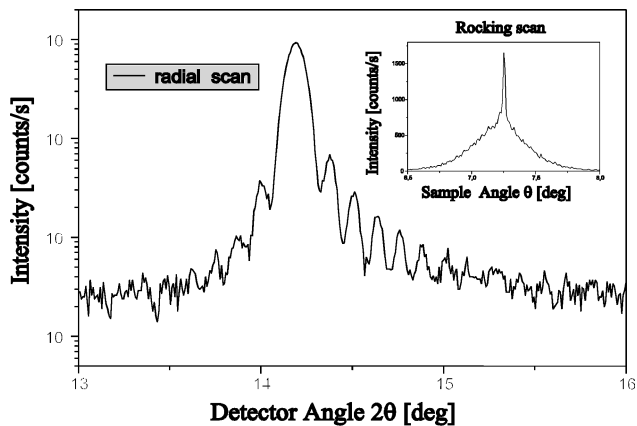


FIG. 3. Radial scan of the Y(0002) reflection. The Bragg peak is accompanied by finite size oscillations, proving the high quality of the film. The inset shows the corresponding rocking scan. It exhibits a two component line shape indicating long range lateral order within the Y(0001) planes.

fore the entire Y film is structurally coherent. The position of the Y(0002) reflection refers to an out of plane lattice constant of 5.75 \AA , which is about 0.3% larger than the bulk value of 5.73 \AA . The rocking curve of the Y(0002) reflection exhibits a two-component line shape with a narrow component superimposed on a broader contribution. Two component line shapes have been observed in other heteroepitaxial systems as well²⁶⁻²⁹ and are a sign for high quality epitaxial growth. The sharp component indicates a long range structural order of the film induced by a flat and monocrystalline substrate, while the broad component reflects short range order fluctuations of individual growth domains. The widths of the two components are 0.018° and 0.4° , respectively.

We have also examined the in-plane epitaxial relation of the Y(0001) film to the Nb(110) buffer layer using surface scattering techniques with glancing incident and exit angles to the surface.^{30,31} The incident angle was kept constant and equal to the critical angle for total external reflection from the surface. The intensity of the exit beam was integrated over a wide range of exit angles via a broad detector window. With this setup the structural information is averaged over the entire thickness. The in-plane detector angle 2θ was fixed to the scattering vector of the Y(11 $\bar{2}$ 0) Bragg peak and the sample is rotated (ω -axis) by 360° around the surface normal. This scan reveals six Bragg reflections equally separated by 60° , reflecting the sixfold symmetry of the (0001) zone axis of Y, as seen in the lower panel of Fig. 4. The varying intensities are due to different geometrical factors such as a tilt of the yttrium planes with respect to the physical surface because of a miscut of the substrate by about 0.5° , which is on the order of the critical angle for total reflection. This leads to different incident angles of the x-ray beam with respect to the crystal planes and causes intensity fluctuations. Keeping the scattering vector constant at the value of the Nb(002) reflection and rotating the sample, two strong Bragg reflections 180° apart can be seen (upper panel of Fig. 4). They originate from the Nb buffer, confirming the twofold symmetry of the Nb(110) layer. The weaker reflections separated by 60° originate from the Nb cap layer. One can distinguish between the buffer and the cap layer by performing x-ray scans at different incident angles of the x-ray

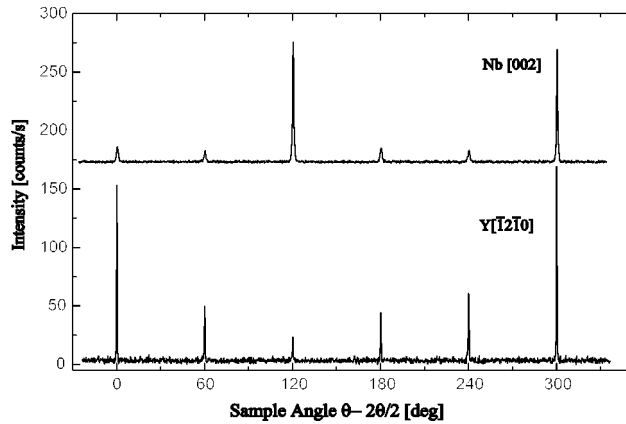


FIG. 4. 360° in-plane rocking scans of the Nb 002 (top) and the Y($11\bar{2}0$) (bottom) reflections, showing that both materials are growing with their in-plane crystal axis parallel to each other. Y grows hexagonal in a single domain on the twofold Nb buffer. The different intensities of the Y reflections stem from geometrical reasons. The strong Nb(002) reflections are due to planes of the Nb buffer layer. The weak Nb(002) reflections originate from the Nb cap layer, showing a sixfold symmetry, due to a Nishiyama-Wassermann epitaxial relationship between Nb(110) and Y(0001). The scans are superimposed on each other for clarity.

beam, probing different depths. With increasing incident angle the intensity of the Nb buffer-reflection increases, whereas the intensity of the cap layer remains constant. The different symmetries for the Nb buffer and the Nb cap can be explained by the different materials they were grown upon. While the $\text{Al}_2\text{O}_3(11\bar{2}0)$ substrate defines a unique in-plane growth direction for the Nb(110) buffer layer, the sixfold Y(0001) surface offers three equivalent directions for the Nb(110) growth. As a result, the cap consists of three domains, separated by 120° . Taking into account the different 2θ values of the Y($\bar{1}2.0$) and the Nb(002) reflections by plotting the intensity versus $\omega = \theta - 2\theta/2$, the niobium reflections coincide exactly with the yttrium reflections, confirming the alignment of the Y($11\bar{2}$) and the Nb(001) planes (Fig. 4).

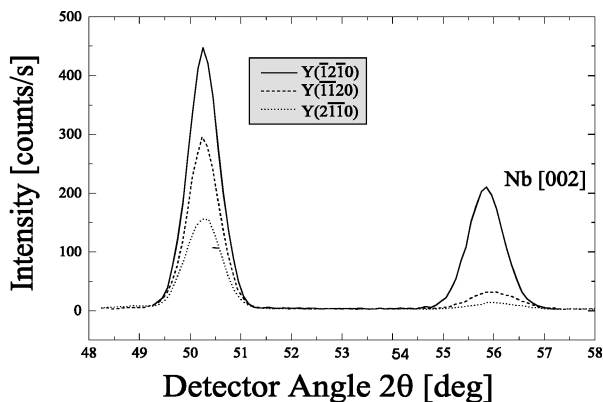


FIG. 5. In-plane radial scans. All equivalent Y($\bar{1}20$) reflections peak at the same position, demonstrating the isotropic growth of Y on Nb. The Nb buffer layer exhibiting a twofold symmetry causes the strong Nb(002) reflection (solid line). The weak Nb(002) reflections originate from the Nb cap layer.

Figure 5 shows in-plane radial scans along three equivalent Y($11\bar{2}0$) directions. All three equivalent Y($11\bar{2}0$) reflections peak at the same 2θ position, indicating that the Y-lattice spacings are isotropic. This is surprising since only one crystallographic axis coincides between Y and Nb, which might have caused an anisotropic pseudomorphic growth of the yttrium layer. The Y($11\bar{2}0$) in-plane reflections exhibit a transverse width of about 0.55° , referring to an in-plane coherence length of about 135 \AA . This is a typical value for epitaxial growth of Nb on Al_2O_3 substrates. Thus the yttrium in-plane domain size is limited by the Nb island size. From the position of the Y peaks we deduce an in-plane lattice parameter of 3.631 \AA , which is slightly smaller than the bulk value of 3.648 \AA . We attribute this slight distortion to the fact that the 3:4 supercell commensuration between Y and Nb is not perfect, as explained above. Note again, that the observed compression of the a axes is isotropic, though the Nb buffer exhibits a strong uniaxial structural anisotropy. The solid line in Fig. 5 represents a scan through the Nb(002) buffer layer peak and the Y($\bar{1}2.0$) peak. Along the Y($\bar{1}2\bar{1}0$) and the Y($2\bar{1}\bar{1}0$) directions no Nb reflection exists from the buffer. The two weak reflections accompanying these Y reflections originate from the Nb cap layer.

The epitaxial relation between Nb(110) and $\text{Al}_2\text{O}_3(11\bar{2}0)$ has been investigated previously and shall not be repeated here. For details we refer to Refs. 32–34.

B. X-ray scattering on the hydrogenated sample

Hydrogen loading at room temperature up to YH_3 degrades slightly the structural long range order of the Y(0001) planes, causing the narrow component in the rocking scan of the unloaded sample to vanish. The $\text{YH}_3(0002)$ rocking curve shows only one broad component with a FWHM of about one degree. The radial scan through the $\text{YH}_3(0002)$ Bragg reflections exhibits the same width and shape as before, indicating a constant coherence length. No additional diffuse scattering from structural disorder could be observed. From the peak position we deduce a c -axis lattice parameter of 6.62 \AA .¹⁴ Within the trihydride phase, the c -axis lattice parameter does not depend on the external hydrogen pressure, i.e., on the hydrogen concentration.

As known from polycrystalline and powder samples, the transition to the hydrate phases affects mainly the c axis. While the c axis expands by about 15%, the change of the basal-plane lattice parameter is only about 0.5%. Epitaxially grown c -axis Y films behave similarly.

The trihydride phase is first observed at a hydrogen pressure of 4 mbar with an in-plane lattice constant of 3.646 \AA , corresponding to an expansion of 0.015 \AA compared to the hydrogen free case. In contrast to the c axis, the in-plane lattice parameter in the trihydride phase changes with hydrogen pressure. Increasing the hydrogen pressure up to 250 mbar, the in-plane lattice constant expands by 0.55% up to 3.651 \AA . We suggest from the different response of the host lattice along the c axis and basal plane directions that the hydrogen sites in the host metal plane are filled last. Within the resolution of the instrument we could not detect any in-plane anisotropy of the lattice expansion.

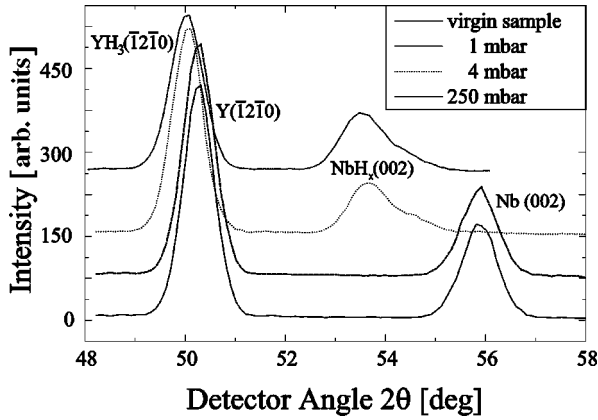


FIG. 6. In-plane radial scans during hydrogen loading at room temperature. The different scans are offset for clarity. The hydrogen concentration increases from the bottom to the top. The stronger in-plane expansion of the Nb buffer layer does not effect the Y symmetry, which is grown on top of it.

In the literature different values for the lattice constants are given. While there is good agreement on an a -axis value of 3.666 ± 0.008 Å, the c -axis value is determined less precisely to 6.629 ± 0.030 Å.^{8,15,35} Our measured values for the lattice constants lie within the error bars of the published data.

The development of the in-plane radial Bragg reflections with increasing hydrogen pressure is represented in Fig. 6. The Y in-plane peak shift only slightly to lower angles while at the same time the Nb in-plane peak shows a large shift due to hydrogen loading. We therefore make the surprising observation that the Y film and Nb buffer expand independently upon hydrogen uptake. The increase of the Nb in-plane lattice parameter by 3.8% within the Nb buffer layer is about 7 times as big as the in-plane lattice expansion of the Y film. The Nb expansion observed here conforms the recently reported expansion of Nb(110) films on sapphire substrates having comparable thickness.³⁶ Moreover, the highly anisotropic in-plane expansion of the Nb buffer layer and its uniaxial structural anisotropy have no effect on the hydrogen uptake in the yttrium film, which expands isotropically in-plane. Thus, the trihydride maintains a sixfold symmetry irrespective to the twofold symmetry of the niobium buffer. There is no sign of a lattice distortion. These two observations indicate weak adhesive forces between or an easy glide plane between the two metals.

The in-plane mosaicity and coherence length remain unchanged during the dihydride to trihydride phase transition. Removing the hydrogen pressure at room temperature, several days are required for the dihydride phase to reappear. Its c -axis lattice constant of 6.00 Å agrees well with the value given in Ref. 8.

C. Neutron reflectivity and isotope exchange

The neutron scattering experiments carried out at ADAM were performed at a 2400 Å thick Y sample, grown in the same way as the sample mentioned above. The higher sample volume was chosen to obtain more scattered intensity. We applied small angle neutron reflectivity methods to determine the hydrogen concentration within the yttrium tri-

hydride phase. In the small angle regime, i.e., at low momentum transfer, neutrons probe the average scattering length density of the sample. Changing the average scattering length density by introducing hydrogen into the sample causes a shift of the critical angle of total reflection. The amplitudes of the finite size oscillations also change as the scattering length density determines the neutron optical contrast. Additionally, the film expands during hydrogenation and the interface roughnesses may be affected. The critical angle of total reflection θ_c of the YH_3 film is related to the hydrogen/yttrium ratio x via

$$\theta_c(x) = \sqrt{\frac{n(x)b(x)\lambda^2}{\pi}}, \quad (1)$$

where the particle density, $n(x)$, is given by $n(x) = (1+x)n_Y$ and the effective scattering length by $b(x) = (b_Y + xb_H)/(1+x)$. Here b_Y and b_H are the coherent scattering lengths for Y and H, respectively, and n_Y is the yttrium particle density (atoms per volume) within the sample. Thus the critical angle θ_c depends on the hydrogen concentration x . In reflectivity scans the measured edge is determined by the layer with the highest scattering length density nb within the sample. As the scattering length density nb for Al_2O_3 is larger than for Y, the critical angle of the virgin sample is determined by the sapphire substrate. Since hydrogen has a negative scattering length, adding hydrogen to the Y film results in a further decrease of nb . Hydrogen in Y is therefore not a suitable isotope for observing changes close to the critical angle as a function of the hydrogen concentration. This can, however, be achieved by replacing hydrogen with deuterium, which has a positive scattering length. As concerns the structure we have not found any difference between H and D in yttrium, except a slight difference in lattice constant, which will be discussed later.

The reflectivity curve of the virgin sample together with a fit to the data is compared with the reflectivity curve of the deuterium loaded sample in Fig. 7. The reflectivity curve of the sample as prepared clearly shows high frequency oscillations which originate from the 2380 Å thick Y layer, as well as oscillations stemming from the 540 Å thick Nb buffer. The fit to the data gives interface roughnesses of about 4 Å. Exposing the sample to a deuterium atmosphere of 100 mbar, the high frequency oscillations vanish and the lower frequency oscillations become damped out quickly as the thickness fluctuations increase strongly. The fit routine based on the Parratt formalism fails under these conditions. The deuterium concentration can still be measured via the critical angle. The edge of total reflection shifts to higher angles as the gas enters the sample (see inset of Fig. 7). The movement of the critical edge stops when the concentration of deuterium within the sample is in equilibrium with the atmosphere surrounding it. A further increase of the pressure has no effect on the position of the critical edge for total reflection, indicating saturation. Longitudinal scans through the Bragg peak assure that the sample has completely converted to the trihydride phase with no reflections left from Y or YD_2 phases. From the measured position of the critical edge of total reflection, we calculated a deuterium concentration of $x = 2.94 \pm 0.03$. Thus the trihydride exhibits a sub-stoichiometric composition. Expelling the deuterium at 472

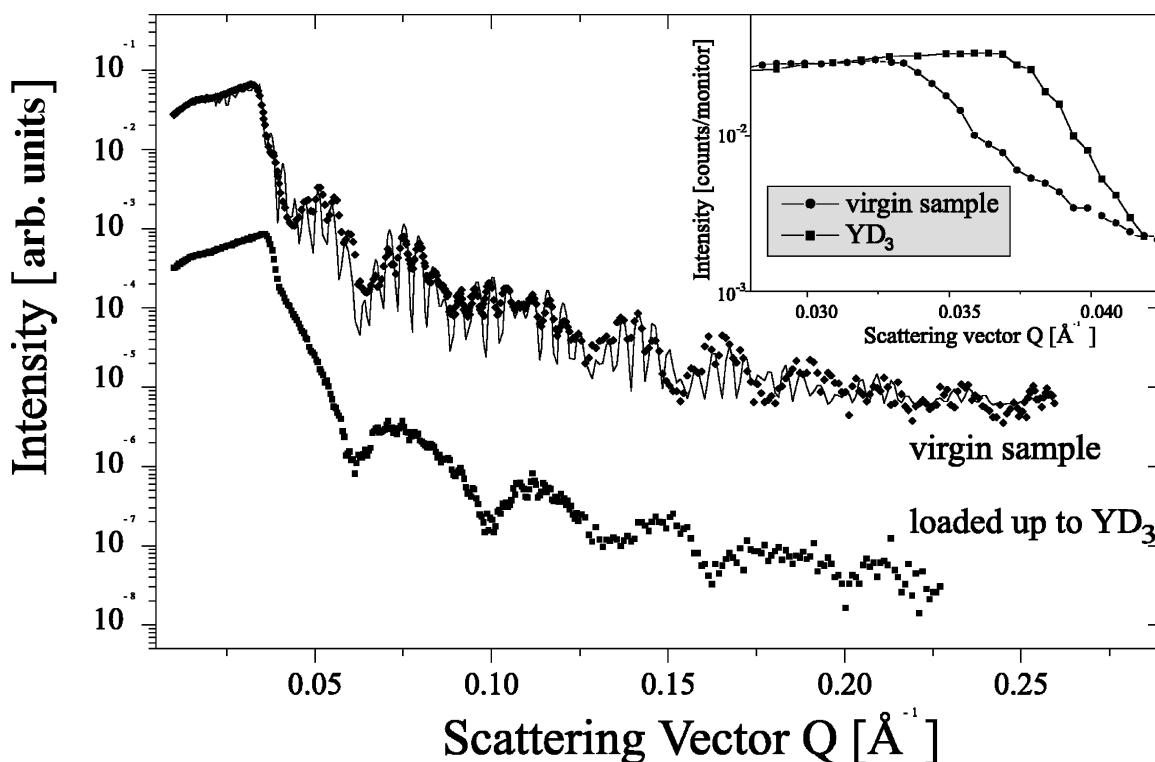


FIG. 7. Small angle reflectivity scans for the sample as prepared (top) and the deuterated sample (bottom), measured with 4.4 \AA neutrons. The solid line is a fit to the scan from the virgin sample, where the critical angle is determined by the sapphire substrate. As the scattering length density increases with increasing deuterium concentration, the critical angle is a measure for the deuterium content of the sample. The inset compares the edges of total reflection in detail.

K, the critical edge of total reflection completely moves back to its initial position. Simultaneously, the (111) reflection of the stable YD_2 reappears in high angle Bragg scans.

With neutron scattering and using the different isotopes the stability of the hydrides can be tested. It is well known that YH_2 is a very stable compound even under vacuum conditions. The heat of formation for YH_2 is relatively high (-114 kJ/mole H),³⁷ indicating a strong hydrogen-metal bond for the hydrogen atoms occupying tetrahedral interstitial sites. In comparison, YH_3 is much less stable and decomposes to YH_2 after removing the hydrogen pressure. If a YD_3 sample is exposed to a hydrogen atmosphere, two different reactions may occur. Either all deuterium atoms will be exchanged by hydrogen atoms, or only those deuterium atoms occupying in and near metal planes with octahedral symmetry.

Neutron diffraction can distinguish between these two cases. The sensitivity of neutrons to the different scattering lengths of the hydrogen isotopes results in distinguishable structure factors. Using the structural parameters determined recently by Udovic *et al.*,¹⁵ the structure factor for the $\text{YH}_3(0002)$ Bragg reflection is given by

$$S_{0002} = \left(\sum_{\alpha} a_{\alpha} b_{\alpha} \exp \frac{-2\pi i}{r_{\alpha}} \right) + b_Y, \quad (2)$$

where a_{α} describes the relative occupation of plane α , b_{α} the average scattering length of the species occupying this plane and r_{α} the relative position of the α plane in units of the distance between two adjacent Y planes. In the case of a stoichiometric composition of YH_3 the occupation number is

1 for the tetrahedral planes and $1/3$ for each in and near metal plane. In model 1, b_{α} was varied continuously from b_D to b_H for all layers simultaneously. In model 2, b_{α} was kept constant at the value of b_D for those planes containing the tetrahedral interstitials. Only b_{α} for the in and near metal planes was varied continuously from b_D to b_H . The first model predicts a decrease in scattered intensity by 20%, while the second model predicts an increase by a factor of four, making the decision between both cases easy.

In Fig. 8 the experimental results are reproduced. We have first measured the intensity at the center of the $\text{YD}_3(0002)$ Bragg reflection under equilibrium deuterium pressure conditions. Then we exchange the deuterium atmosphere of 100 mbar by a hydrogen atmosphere of the same pressure at room temperature. The intensity of the Bragg peak stays constant. Obviously there is no interchange taking place with the deuterated sample and the hydrogen atmosphere at this temperature and during the observation time. At 472 K and after 12 minutes the neutron count rate starts to decrease and reaches a new stable plateau of about 78% of the initial value. Radial scans through the $\text{YD}_3(0002)$ reflection before isotope exchange and the $\text{YH}_3(0002)$ reflection after completion of the isotope exchange show two respective peaks which coincide in position and width but which differ in integrated intensity by 21.5%. The same behavior can be observed in transverse scans. The exchange of deuterium and hydrogen is fully reversible, the intensity change could be reproduced several times. After each exchange, the concentration of deuterium and hydrogen was checked by small angle neutron reflectivity to assure that the isotope

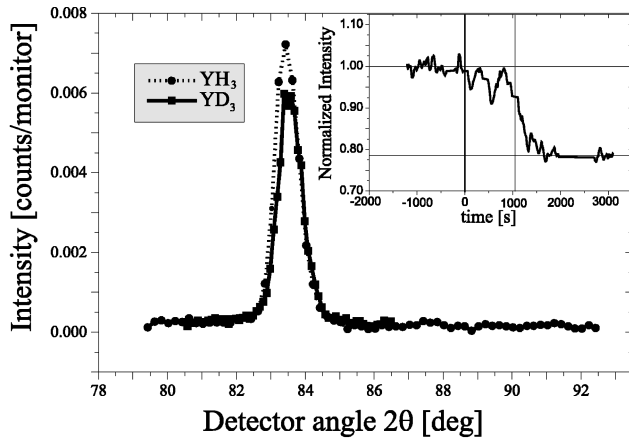


FIG. 8. Comparison of the YD_3 reflection with the YH_3 reflection. Exchanging the hydrogen isotope, the integrated intensity drops to 78.5% of the starting value. The inset shows the development of the peak intensity of the (0002) reflection during the transition from YD_3 to YH_3 . At $t=0$ s the temperature was set to 372 K; at $t=1050$ s the temperature was increased to 472 K. The inset compares the YD_3 reflection with the YH_3 reflection.

exchange has indeed taken place. Within the YH_3 phase the critical angle of total reflection is always determined by the sapphire substrate, obscuring the sensitivity for the hydrogen content. On the other hand, the sensitivity to the deuterium concentration is not limited and we have always measured a deuterium concentration of $x=2.94$, even after several hydrogen-deuterium cycles, indicating a complete isotope exchange.

As the intensity difference of the (0002) Bragg peak between YD_3 and YH_3 is very sensitive to x , the observed decrease in intensity is a measure of the hydrogen concentration. While a stoichiometric composition leads to an intensity decrease by 20% upon isotope exchange, for a sub-stoichiometric composition of $x=2.8$ we calculate a decrease of 49%. From our measured decrease to 78.5% we calculated a deuterium concentration of $x=2.99\pm 0.03$, which is a higher concentration than calculated from the small angle reflectivity curve. This difference may be attributed to two different effects. Either there is a nonhomogeneous distribution of hydrogen and deuterium in the sample, or the isotope exchange is not quite complete. In the first case the critical angle for total reflection, being sensitive to the average concentration in the yttrium film, would give a different result than the Bragg peak intensity, which probes only the ordered, crystalline part of the sample. If this concept applies, we conclude that the hydrogen concentration within the ordered regions of the film reaches $x=2.99$, while it is less in other regions of the sample, such as grain boundaries, etc. lowering the overall hydrogen content in the sample. At the present time we cannot distinguish between one or the other model, and further experiments are necessary. In any case, exploiting the scattering contrast of the different hydrogen isotopes offers an independent method to determine the hydrogen concentration if the structure is known. Vice versa, if the concentration is known, the structural model can be refined.

There is another effect which is worth mentioning. The $YD_3(0002)$ Bragg peak is slightly shifted towards higher

angles with respect to the YH_3 Bragg reflection, indicating a smaller lattice spacing within YD_3 as compared to the YH_3 structure. This isotope effect agrees well with the lattice constants published in Ref. 8. Again, the epitaxially grown film shows no difference in the structural properties as polycrystalline or powder samples.

D. Off-specular neutron diffraction

While the previously discussed measurements along the specular rod provide information about the layered structure of the sample, they are not sensitive to the lateral arrangement of the atoms within the individual layers. In order to study the change of the stacking sequences during the phase transitions as well as the in-plane deuterium ordering, scans along reciprocal lattice rods containing in-plane components were carried out.

The sample used in this experiment was prepared in the same manner as the samples used in the previous experiments. However, the Pd cap layer was rather thin and did not completely cover the underlying Y film. Therefore parts of the sample were oxidized. Below the uncovered parts of the sample almost no deuteration takes place as the natural oxide layer prevents the uptake of deuterium. Deuteration of these parts of the sample requires lateral diffusion of deuterium entering at Pd-covered parts. During the time the experiment was carried out, deuteration by lateral diffusion was negligible. Thus the phase transition was not complete. This sample composition allows always to observe Bragg reflections emerging from deuterium free yttrium, which serve as markers in reciprocal space.

The bottom panel in Fig. 1 shows schematically the real space of the hexagonal basal plane of Y. To simplify the description of the following measurements, three perpendicular axes were chosen to characterize the hexagonal lattice. In this description the $Y(11\bar{2}0)$ axis is called the H axis, and the perpendicular in-plane direction $(1\bar{1}00)$ is called the K direction. The specular c axis coincides with the L axis. The first allowed in-plane reflections will be denoted as (100) and (010), respectively. As demonstrated by the GIXRD measurements, the basal plane maintains its sixfold symmetry during hydrogenation. In the cubic coordinates of the YD_2 phase, the H direction coincides with the $(1\bar{1}0)$ direction, the K direction with the $(11\bar{2})$ direction and the L direction with the closed packed (111) direction.

As a consequence of the structural changes during the transition to the β phase, the reciprocal space changes as well. Figure 9 shows the K-L plane in reciprocal space. Reflections which are only allowed in the hexagonal lattice are marked with hexagons, reflections which are only allowed in the fcc lattice are indicated by squares. Common reflections are represented by circles. Due to the $ABCABC\dots$ stacking, the reciprocal space of a fcc lattice in the K-L plane is not symmetric with respect to L or K. Domains which are rotated by 180° against each other will produce two sets of reflections which are distinguished by open and solid squares in Fig. 9. There is *a priori* no reason for preferring one orientation. Thus scans along (01L) do not only show the different stackings, they are sensitive to different domains as

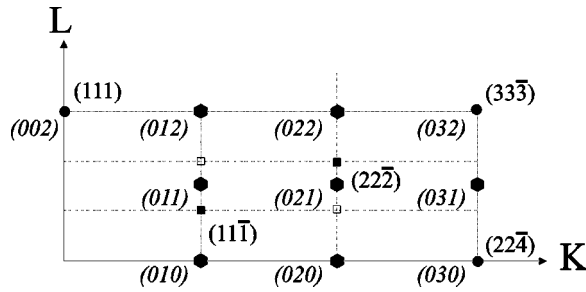


FIG. 9. Reciprocal lattice of the K-L plane. Allowed hexagonal reflections are represented by bold hexagons and indexed in italics. Bold and open squares mark the allowed positions of the two possible fcc domains, of which only one (bold symbols) is indexed. Common reflections are represented by circles.

well. The relative intensities of the fcc reflections along this rod are a measure for the scattering volume of the two possible domain orientations.^{38,39}

To follow the phase transitions during deuteration, scans along (00L) were carried out. In reciprocal space units of the hydrogen free Y lattice, the reflections of Y, YD₂, and YD₃ appear at L=2, L=1.91, and L=1.74, respectively.

Scans along the (01L) direction are shown in Fig. 10. The virgin sample exhibits a strong reflection at (011) which slightly shifts to lower L values during deuteration in the alpha phase. A further increase of the gas pressure leads to a drastic decrease of its intensity. However, it does not vanish completely as the phase transition does not take place in the entire sample as described above. At the same time two new reflections occur at L=0.64 and L=1.28, which is one third and two thirds of L=1.91. The strongly reduced intensity of the hexagonal peak and the appearing cubic reflections clearly show that the lattice expansion during the α - β transition is accompanied by a rearrangement of the stacking sequence. Furthermore, the occurrence of both fcc reflections indicates that within the sample both possible stackings ABC... and BAC... are realized. The intensity ratio of 1:3 of these two reflections agrees well with the intensity ratio of measured powder spectra. There seems to be no preferred orientation of the fcc stackings. Obviously, as the sample undergoes the hcp-fcc transition, the probability for formation of either domain is equal. This observation agrees

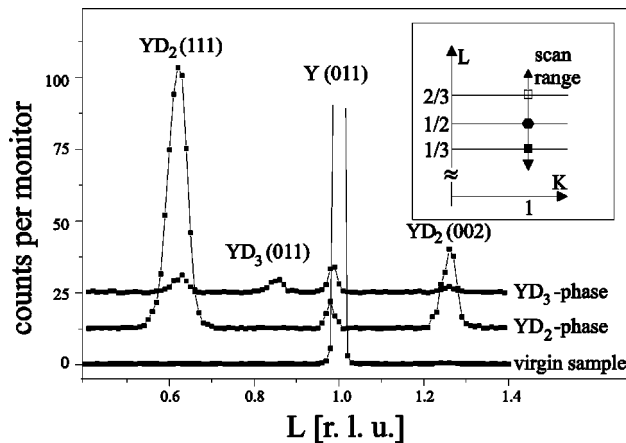


FIG. 10. Scans along (01L) for Y (top), YD₂ (middle), and YD₃ (bottom).

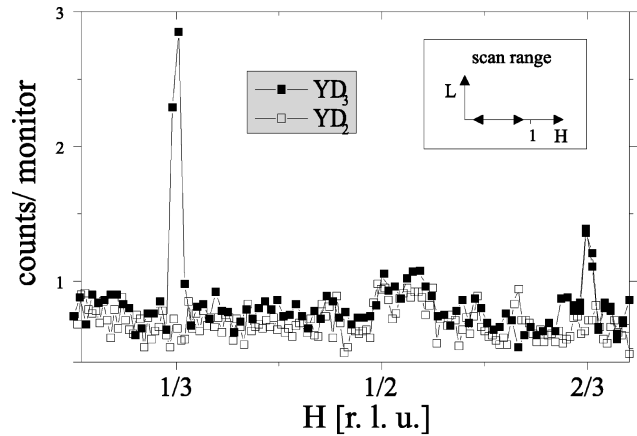


FIG. 11. Scans along (H00) for YD₂ (open symbols) and YD₃ (bold symbols). The peaks at H=1/3 and 2/3 in the trihydride phase show that the deuterium distribution exhibits a wavylike modulation about the Y basal planes in the [100] direction corresponding to the hexagonal [112̄0] direction.

with recent x-ray photoelectron diffraction measurements on yttrium films grown on tungsten.⁴⁰

A further increase of the deuterium pressure causes the fcc reflections to drop in intensity as the sample reaches the YD₃ phase. Again, the phase transition is not complete. Within the YD₃ phase a weak Bragg reflection at L=0.87 (=1.74/2) can be observed, originating from the YD₃(011) reflection. In contrast to the P3 structure of the virgin metal, YD₃ crystallizes in the higher symmetry $P\bar{3}c1$ structure, for which only even L reflections exhibit strong intensity. Expelling the deuterium, the reflection at L=0.87 vanishes and the reflections at L=0.64 and L=1.28 reappear. The sample was cycled three times without any measurable loss of structural coherence.

Like the transition from Y to the dihydride phase, the transition from the dihydride phase to the trihydride phase is accompanied by a rearrangement of the stacking sequence along the closed packed axis. The hexagonal c axis of YD₃ coincides with the c axis of the virgin metal. This is, however, by no means obvious. The fcc structure of YD₂ has four equivalent (111) axes, and single crystals of YD₃ develop domains along all four directions. This is because the sixfold symmetry of the Y c axis does not provide a template for a particular {111} axis in the YD₂ phase. Then one would expect four different YD₃ domains with their c axis to align along the {111} of the fcc structure. In thin films the situation is different. A thin film can easily relax along the growth direction which in this case coincides with only one of the four (111) directions. This direction will be the direction of choice if a structural phase transition requires an uniaxial lattice expansion.

Within the trihydride phase, scans along (H00) and (H02) exhibit Bragg reflections at H=±1/3 and H=±2/3, as shown in Fig. 11. They do not occur in x-ray diffraction measurements. Since those reflections are absent for the virgin sample as well as for YD₂, they clearly show the ordering of the deuterium atoms within the metal. As there are no additional reflections along K or L, we conclude that thin single crystalline films, like powder samples exhibit a uniaxial deuterium modulation along the H direction. This

modulation is commensurate with respect to the metal lattice. The modulation length equals three times the distance of the yttrium atoms in this direction. As in previously measured NPD spectra, superstructure reflections appear only at (H0L) where $L=2n$ for integer values of n .

As band structure calculation based on this structure do not predict the metal insulator transition, Kelly *et al.*²⁰ suggested a lower-energy, broken-symmetry ($P3$) structure for thin YD_3 films. In this assumption the ($P3$) structure would be stabilized by epitaxial strain in thin films.⁴¹ The symmetry lowering would result in additional Bragg reflections which are forbidden in the high-symmetry structure. In contrast to the ($P\bar{3}c1$) structure, in which the c -glide symmetry restricts the allowed Bragg reflections to (H0L) for even values of L , the absence of this element of symmetry in the ($P3$) structure abolishes this restriction. We could not find any (H0L) reflection for odd values of L , indicating that the ($P\bar{3}c1$) is preserved for epitaxial YD_3 films. In all structural measurements which we carried out so far, there is no contradiction to the ($P\bar{3}c1$) structure.

IV. CONCLUSION AND SUMMARY

Epitaxial single crystalline Y(0001) films with perfect six-fold symmetry have been grown on a Nb(110)/ Al_2O_3 (11 $\bar{2}$ 0) buffer/substrate system with uniaxial structural symmetry. While this system has often been grown in conjunction with rare-earth superlattices,^{42,43} we present here a complete structural analysis of the in-plane epitaxial relation between the different layers. More surprising than the hexagonal symmetry of the virgin Y(0001) layer is the fact that the symmetry and epitaxial relation is maintained during hydrogen uptake and lattice expansion to the bulk stoichiometry of YH_3 . Admittedly, the lattice expansion is highly anisotropic and takes place mostly in the out-of-plane direction. Nevertheless, the 0.5% in-plane lattice expansion of Y is surprisingly isotropic irrespective of the simultaneously expanding Nb buffer layer to a much larger value of 3.8%, and irrespective

of the different in-plane structural symmetries.

The structural transition from the pure Y to the YH_2 phase causes some degradation of the structural coherence, indicated, for instance, by the loss of the sharp component in the transverse scan across the (0002) peak. Between the YH_2 and the YH_3 phase no further loss in structural coherence is observed and the phase transitions are completely reversible.

With small angle neutron reflectivity measurements as well as high angle neutron scattering experiments we have investigated the isotope exchange in YH_3 and possible preferential occupation sites with stronger binding energies. The results show that there is no doubt that all hydrogen atoms are being exchanged by deuterium (and vice versa) within the sample by changing the surrounding gas atmosphere. The position of the critical angle for total reflection of neutrons as well as the intensity of the (0002) Bragg peak can be shifted continuously between the two limiting values of YH_3 and YD_3 depending on the relative H/D ratio in the sample. This isotope exchange takes place on a rather short time scale of only a few minutes.

Off specular neutron diffraction demonstrates nicely the reorientation of the stacking sequence of the yttrium atoms during the phase transition. It also shows the wavelike modulation of the deuterium atoms in the basal plane of YD_3 . All Bragg reflections are in agreement with the $P\bar{3}c1$ structure found in powder samples. No additional reflections, indicating a broken symmetry, could be found. There seems to be no structural difference between thin epitaxial films and bulk samples.

ACKNOWLEDGMENTS

We would like to thank R. Griessen, R. Kirchheim, and B. Hjörvarsson for fruitful discussions. This work was supported by the Bundesministerium für Bildung und Forschung under Contracts No. ZA4BC1 and No. ZA4BC2 and the EU-TMR project Metal-hydride films with switchable physical properties (ERB FMRX-CT98-187), which we gratefully acknowledge.

¹Y. Fukai, *The Metal-Hydrogen System* (Springer-Verlag, Berlin, 1993).

²*Hydrogen in Metals*, edited by G. Alefeld and J. Vökl (Springer-Verlag, Berlin, 1978), Vols. I and II.

³*Hydrogen in Intermetallic Compounds*, edited by L. Schlapbach (Springer-Verlag, Berlin, 1988), Vols. I and II.

⁴F. Klose, Ch. Rehm, D. Nagengast, H. Maletta, and A. Weidinger, *Phys. Rev. Lett.* **78**, 1150 (1997).

⁵B. Hjörvarsson, J. A. Anderson, P. Isberg, T. Watanabe, T. J. Udovic, G. Anderson, and C. F. Majkrzak, *Phys. Rev. Lett.* **79**, 901 (1997).

⁶F. Stillesjö, B. Hjörvarsson, and H. Zabel, *Phys. Rev. B* **54**, 3079 (1996).

⁷G. Song, A. Remhof, K. Theiss-Bröhl, and H. Zabel, *Phys. Rev. Lett.* **79**, 5062 (1997).

⁸P. Vadja, in *Handbook on the Physics and Chemistry of Rare Earths*, edited by K. A. Gschneidner and L. Eyring (Elsevier, Amsterdam, 1995), Vol. 20.

⁹J. N. Huiberts, R. Griessen, J. H. Rector, R. J. Wijngarten, J. P. Dekker, D. G. de Groot, and N. J. Koeman, *Nature (London)* **380**, 231 (1996).

¹⁰O. Blaschko and G. Krexner, *Phys. Rev. Lett.* **55**, 2876 (1985).

¹¹I. S. Anderson, N. F. Berk, J. J. Rush, T. Udovic, R. G. Barnes, A. Magerl, and D. Richter, *Phys. Rev. Lett.* **65**, 1439 (1990); **57**, 2822 (1986).

¹²P. Vadja and J. N. Daou, *Phys. Rev. Lett.* **66**, 3176 (1991).

¹³P. van der Sluis, M. Ouwkerk, and P. A. Duine, *Appl. Phys. Lett.* **78**, 1315 (1997).

¹⁴A. Remhof, G. Song, K. Theiss-Bröhl, and H. Zabel, *Phys. Rev. B* **56**, R2897 (1997).

¹⁵T. J. Udovic, Q. Huang, and J. J. Rush, *J. Phys. Chem. Solids* **57**, 423 (1996).

¹⁶Y. Wang and M. Y. Chou, *Phys. Rev. B* **51**, 7500 (1995).

¹⁷Y. Wang and M. Y. Chou, *Phys. Rev. Lett.* **71**, 1226 (1993).

¹⁸J. P. Dekker, J. van Ek, A. Lodder, and J. N. Huiberts, *J. Phys.: Condens. Matter* **5**, 4805 (1993).

- ¹⁹K. K. Ng, F. C. Zhang, V. I. Anisimov, and T. M. Rice, Phys. Rev. Lett. **78**, 1311 (1997).
- ²⁰P. J. Kelly, J. P. Dekker, and R. Stumpf, Phys. Rev. Lett. **78**, 1315 (1997).
- ²¹J. Kwo, M. Hong, and S. Nakahara, Appl. Phys. Lett. **49**, 319 (1986).
- ²²A. Abromeit, R. Siebrecht, G. Song, H. Zabel, F. Klose, D. Nagengast, and A. Weidinger, J. Alloys Compd. **253-254**, 58 (1997).
- ²³R. Siebrecht, A. Schreyer, U. Englisch, U. Pietsch, and H. Zabel, Physica B **241-243**, 169 (1998).
- ²⁴L. G. Parratt, Phys. Rev. **95**, 359 (1954).
- ²⁵P. Bödeker, A. Abromeit, K. Bröhl, P. Sonntag, N. Metoki, and H. Zabel, Phys. Rev. B **47**, 2353 (1993).
- ²⁶P. M. Reimer, H. Zabel, C. P. Flynn, and J. A. Dura, Phys. Rev. B **45**, 11 426 (1992).
- ²⁷A. Gibaud, R. A. Cowley, D. F. McMorrow, R. C. C. Ward, and M. R. Wells, Phys. Rev. B **48**, 14 463 (1993).
- ²⁸P. F. Miceli, in *Semiconductor Interfaces, Microstructures and Devices: Properties and Applications*, edited by Z. C. Feng (Adam Hilger, IOP Publishing Ltd., Bristol, 1992).
- ²⁹B. Wölfing, Diploma thesis, Ruhr-Universität Bochum, 1998.
- ³⁰R. Feidenhans'l, Surf. Sci. Rep. **10**, 105 (1989).
- ³¹H. Dosch, *Critical Phenomena at Surfaces and Interfaces* (Springer-Verlag, Berlin, 1992).
- ³²J. Mayer, C. P. Flynn, and M. Rühle, Ultramicroscopy **33**, 51 (1990).
- ³³P. Sonntag, W. Donner, N. Metoki, and H. Zabel, Phys. Rev. B **49**, 2869 (1994).
- ³⁴G. Gutekunst, J. Mayer, and M. Rühle, Philos. Mag. A **75**, 1329 (1997).
- ³⁵M. Mansmann and W. E. Wallace, J. Phys. (Paris) **25**, 254 (1964).
- ³⁶G. Song (private communication).
- ³⁷L. N. Yannopoulos, R. K. Edwards, and P. G. Wahlbeck, J. Phys. Chem. **69**, 2510 (1965).
- ³⁸F. Frey, W. Prandl, J. Schneider, C. Zeyen, and K. Ziebeck, J. Phys. F **9**, 603 (1979).
- ³⁹T. Sebastian and P. Krishna, Phys. Status Solidi A **101**, 329 (1987).
- ⁴⁰J. Hayoz, S. Sarbach, Th. Pillo, E. Boschug, D. Naumovic, P. Aebi, and L. Schlapbach, Phys. Rev. B **58**, R4270 (1998).
- ⁴¹P. J. Kelly, J. P. Dekker, and R. Stumpf, Phys. Rev. Lett. **79**, 2921 (1997).
- ⁴²C. F. Majkrzak, J. Kwo, M. Hong, Y. Yafet, D. Gibbs, C. L. Chien, and J. Bohr, Adv. Phys. **40**, 99 (1991).
- ⁴³C. P. Flynn and M. B. Salamon, in *Handbook of the Physics and Chemistry of Rare Earths*, edited by K. A. Gschneider, Jr. and L. Eyring (Elsevier Science, North-Holland, Amsterdam, 1996), Vol. 22.